Earth and Planetary Science Letters 620 (2023) 118323

Contents lists available at ScienceDirect

Earth and Planetary Science Letters

journal homepage: www.elsevier.com/locate/epsl

Tracking changes in magma transport from very-long-period seismic signals at Piton de la Fournaise volcano

Zacharie Duputel [a,b,*], Valérie Ferrazzini [a,b], Cyril Journeau [c,d], Philippe Catherine [a,b], Philippe Kowalski [a,b], Aline Peltier [a,b]

[a] Observatoire Volcanologique du Piton de la Fournaise, Institut de Physique du Globe de Paris, La Plaine des Cafres, France
[b] Université Paris Cité, Institut de Physique du Globe de Paris, CNRS, Paris, France
[c] Institut des Sciences de la Terre, Université Grenoble Alpes, CNRS (UMR 5275), Grenoble, France
[d] Department of Earth Sciences, University of Oregon, Eugene, OR, USA

ARTICLE INFO

Article history:
Received 6 March 2023
Received in revised form 29 June 2023
Accepted 22 July 2023
Available online 28 August 2023
Editor: C.M. Petrone

Keywords:
volcano seismology
Piton de la Fournaise
VLP events
dike geometry

ABSTRACT

Changes in magma properties and transport geometry can have a direct impact on volcanic activity. However, such variations can be difficult to track during eruptions. We report previously undetected very-long-period (VLP) signals at Piton de la Fournaise that can be used to probe changes in magma transport. Source analysis of VLP events during the August-October 2015 eruption indicates a source depth of about 0.9 -1.2 km and points to the resonance of the magma dike feeding the eruption. The evolution of the resonance period reveals a shortening of the dike when the magma flux decreases at the end of the eruption. VLP events are actually quite frequent at Piton de la Fournaise: all eruptions analyzed in this study exhibit VLP signals that are indicative of rapid drops in lava discharge. This work encourages the detection of VLP signals to monitor changes in magma flow during volcanic eruptions, and anticipate the corresponding evolution in effusive activity.

1. Introduction

The Piton de la Fournaise volcano (La Réunion island) is one of the most active and best monitored volcanoes in the world, with more than two eruptions per year since 1998 and a dense monitoring network of about 100 geophysical and geochemical stations (Chevrel et al., 2021; Peltier et al., 2020; Roult et al., 2012; Staudacher and Peltier, 2016). The morphology of the Piton de la Fournaise edifice is marked by a 10 km wide caldera known as the "Enclos Fouqué", in the middle of which a terminal cone reaches an altitude of 2632 m (Fig. 1). The terminal cone (i.e., the volcano's central cone) stands over a magma reservoir located at about sea level (Peltier et al., 2012) and is overlooked by a 1 km wide summit caldera ("Cratère Dolomieu"). Seismic activity at Piton de la Fournaise is mostly clustered in swarms of volcano-tectonic earthquakes located below the terminal cone before eruptions (Duputel et al., 2021; Sapin et al., 1996). These pre-eruptive volcano-tectonic seismic swarms mark the onset of dike injections from the shallow magma reservoir (Duputel et al., 2019). These rapid increases of seismicity accompanied with large deformation rates during magma injections allow to anticipate eruptions (Beauducel et al., 2020; Peltier et al., 2020; Roult et al., 2012): since the establishment of the volcano observatory in 1979, all 83 eruptions of Piton de la Fournaise have been forecasted (Peltier et al., 2022). Furthermore, with the improvement of seismic and geodetic networks over the last two decades, it is now possible to track magma migration towards the surface, giving early indications on the location of future eruption sites (Beauducel et al., 2020; Duputel et al., 2019; Journeau et al., 2020; Smittarello et al., 2019; Taisne et al., 2011).

Despite advances in volcano monitoring, it is currently difficult to forecast when an eruption will end. In terms of volcanic hazard, this is equally important as predicting future eruptions, because the eruptive duration largely controls the spatial extent of lava flows downslope of eruptive vents (Chevrel et al., 2022). Part of the challenge lies in the difficulty of monitoring the evolution of magma properties and dike geometry during eruptions. Magma discharge rate can be quantified in near real time from satellite data and volcanic tremor amplitude (Coppola et al., 2009; Hibert et al., 2015). Using such observations, it is possible to predict the end date of eruptions by assuming that they are fed by a single magma reservoir releasing its elastic strain energy as it re-equilibrates with the lithostatic pressure (Bonny and Wright, 2017; Wadge, 1981).

* Corresponding author at: Observatoire Volcanologique du Piton de la Fournaise, 14 RN3 Km 27, 97418 La Plaine des Cafres, La Réunion, France.
E-mail address: duputel@ipgp.fr (Z. Duputel).

https://doi.org/10.1016/j.epsl.2023.118323
0012-821X/

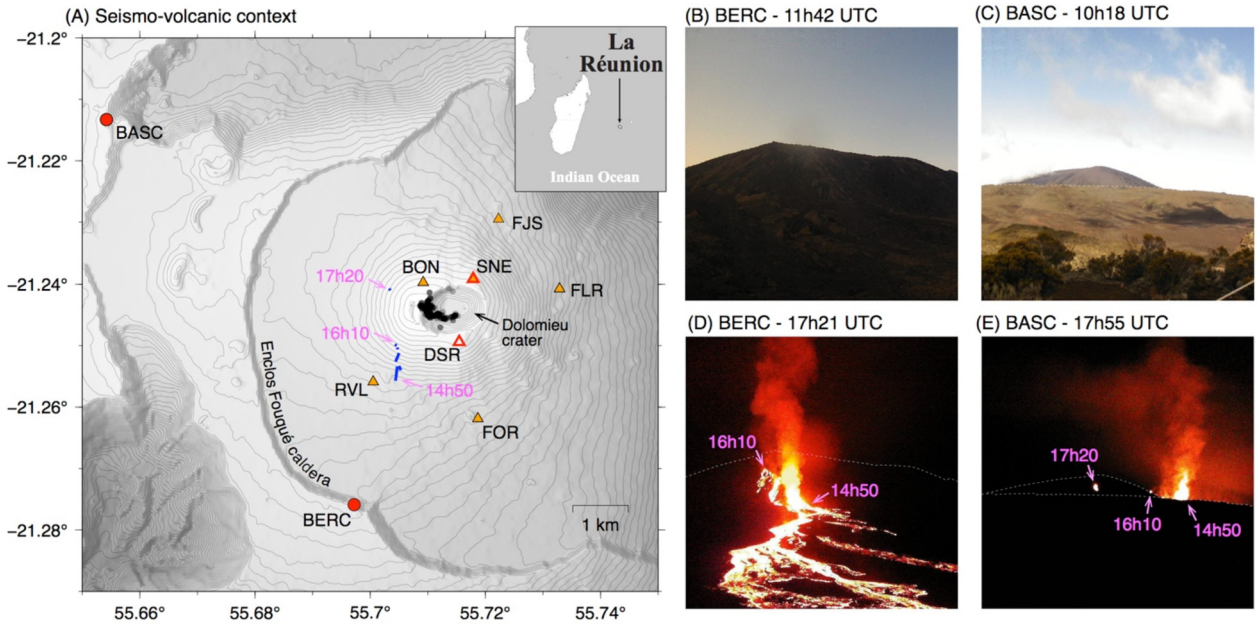

Fig. 1. The August-October 2015 eruption at Piton de la Fournaise. (**A**) Seismo-volcanic context. Blue lines indicate the location of eruptive fissures. Black circles are earthquake locations during the volcano-tectonic swarm preceding the eruption. Orange and red triangles indicate the location of seismic and GNSS stations used in this study, respectively. Station SNE includes a seismometer, a tiltmeter and a GNSS antenna. Red circles show the camera locations whose pictures are shown on the right. Pink labels indicate the onset times of eruptive fissures activity (UTC times on August 24). (**B**)-(**C**) Photos taken by the camera stations BERC and BASC the day before the eruption. (**D**)-(**E**) Photos taken after the onset of the eruption. Dashed lines outline topographic features visible in daytime photos (terminal cone and rim of the Enclos Fouqué caldera).

Although such forecast performs well for short lived eruptions at Piton de la Fournaise (Bonny and Wright, 2017), it does not work for longer eruptions that are associated with more complicated time-evolutions (Coppola et al., 2009). Beyond the simple elastic model of magma release, there are additional processes controlling the eruptive histories. By combining discharge rate estimates with geodetic data and the analysis of erupted products, it has been showed that long-lasting eruptions can be drawing magma from increasingly deeper storage zones, which can drive effusive paroxysms at the end of eruptions (Coppola et al., 2017). In addition, the geometry of magma conduits can change significantly during eruptions. Eruptive activity at Piton de la Fournaise usually evolves from lava fountains and flows discharged along elongated fissures to the focus of emissions on a localized vent, over timescales ranging from hours to a few days (Fukushima et al., 2010). This channelization into a small number of eruptive vents was also observed at other volcanoes (Jones et al., 2017; Keating et al., 2008; Wylie et al., 1999). For example, the 1959 summit eruption at Kilauea volcano (Hawaii) began as a 800 m long fissure, which focused to a single vent within a day (Richter et al., 1970). Similar observations have been reported in Iceland, for instance during the 1973 Heimaey island eruption and more recently during the 2014 Bárðarbunga eruption (Witt et al., 2018; Wylie et al., 1999). Dikes that supply such eruptions also evolve at depth and begin to partially solidify, resulting in a shortening of the dike width. Apart from numerical and laboratory experiments (Bruce and Huppert, 1989; Pansino et al., 2019), very few constraints exist on the evolution of magmatic dike geometries during eruptions.

Very-long-period (VLP) signals with periods ranging from 2 to 100 s are observed at many volcanoes and are often attributed to transient perturbations in the magma flow (Chouet and Matoza, 2013). Due to their very long wavelengths, these waveforms are not strongly affected by volcano structural heterogeneities and provide invaluable constraints on dike and magma properties that are not readily accessible with other observations. Inversions of VLP waveforms have imaged various dike, sill and conduit geometries along with more complicated configurations (Aster et al., 2003; Cesca et al., 2020; Chouet and Matoza, 2013; Kumagai et al., 2003; Legrand and Perton, 2022; Liang et al., 2020; Niu and Song, 2021; Ohminato et al., 1998). When such events occur in a repetitive fashion, they can also be used to track the time evolution of magma properties and transport (Crozier and Karlstrom, 2022; Kumagai, 2006). Only few long-period (LP) and very-long-period (VLP) events have been previously reported at Piton de la Fournaise (Aki and Ferrazzini, 2000; Duputel and Rivera, 2019; Fontaine et al., 2019; Zecevic et al., 2013). A rare instance was during the 2007 summit caldera collapse, during which we observed VLP signals associated with the sudden drop of the caldera floor in the magma reservoir (Duputel and Rivera, 2019; Fontaine et al., 2019). At the time of the 2007 collapse, the only broadband station available in the vicinity of the volcano was the Geoscope station RER, located 8 km away from the summit. The monitoring network has considerably evolved since then and is now equipped with 29 broadband stations, allowing a wide range of signals to be recorded (Observatoire Volcanologique Du Piton De La Fournaise (OVPF) and Institut De Physique Du Globe De Paris (IPGP), 2008).

Here, we report syn-eruptive VLP signals at the Piton de la Fournaise. These signals correspond to the resonance of a magma-filled crack during the August-October 2015 eruption and can be used to track the time-evolution of the dike geometry feeding the eruptive site. Although VLP events can be hidden by the eruptive tremor, they are clearly visible when filtering seismic data at long period. We show that similar VLP signals can be detected during several other volcanic eruptions at Piton de la Fournaise.

2. Methods and results

2.1. Chronology of the August-October 2015 eruption

The eruption that started on 24 August 2015 at Piton de la Fournaise was preceded by an intense seismic swarm of more than one thousand volcano-tectonic (VT) earthquakes indicating the onset of a magmatic intrusion 2 hours before it reached the surface (Duputel et al., 2019). The location of VT earthquakes beneath the southwestern rim of the Dolomieu crater (Fig. 1) suggests that the magma injection initiated within the region above the magma

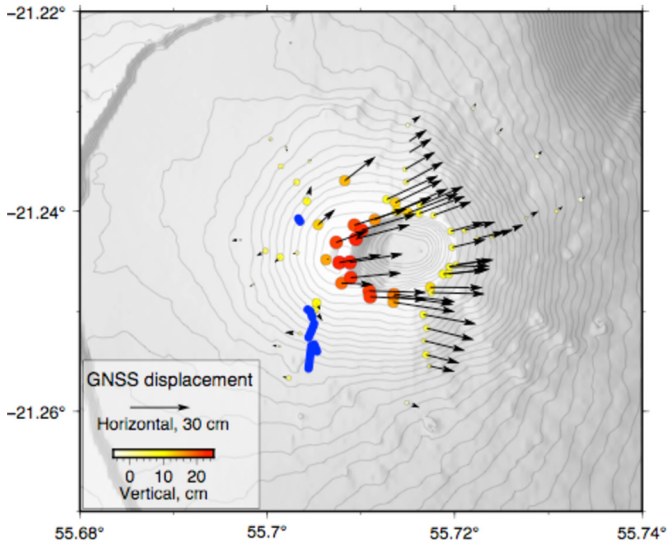

Fig. 2. Displacement field induced by the August-October 2015 eruption. Vectors and colored circles indicate horizontal and vertical GNSS displacements, respectively. Blue lines indicate the location of eruptive fissures (also shown in Fig. 1).

reservoir at ~2 km depth below the surface (details about VT events detection and relocations are provided in the supplementary Text S1). This is confirmed by GNSS displacements (Fig. 2) that are consistent with the propagation of a subvertical dike in the southwest flank of the terminal cone (GNSS data processing is described in the supplementary Text S2). Note that the displacement field in Fig. 2 is asymmetric with a large eastward motion east of the eruptive fissure. Assuming a linear elastic homogeneous medium, inversion of InSAR data for the August-October 2015 eruption suggested that such asymmetry could be explained by a curved intrusion (Dumont et al., 2022). Such preferential motion of the eastern flank is systematic at Piton de la Fournaise and other interpretations have been proposed such as an elasto-plastic behavior of the edifice or the existence of a décollement fault below the eastern flank (Dumont et al., 2022; Got et al., 2013).

After a migration of about 2 hours, the dike finally erupted by intersecting the terminal cone, first on its southern flank at 14:50 UTC and 30 min later at higher elevation on its northern flank (Fig. 1 and supplementary Movies S1 and S2). The activity later focused on the southernmost eruptive fissure, ultimately leading to the formation of the "*Piton Kalla et Pélé*" eruptive vent. In this study, we monitored eruptive activity using Time Averaged lava Discharge Rate (TADR) time-series converted routinely from MODIS-derived spectral radiance data provided by the MIROVA hot spot detection system (Coppola et al., 2017, 2009). These measurements shown in Fig. 3 have an uncertainty of +/-35% depending on the eruptive conditions (topography, eruptive style, etc.). We also monitored the eruptive tremor amplitude using vertical records of the RVL broadband station, located a few hundred meters from the eruption site (Fig. 1A). We computed the mean absolute amplitude over 1 min sliding time-windows after deconvolution from the instrument response and band-pass filtering in the 2-4 Hz frequency band (Fig. 3). After two months of continuous activity, the end of the eruption was marked by two pauses on October 18-22 and 24-29, during which lava emissions completely ceased before resuming abruptly. The eruption finally stopped on October 31, 2015.

2.2. VLP signals

About 40 minutes after the onset of the eruption, a swarm of VLP events began to be recorded at seismic stations near the terminal cone. Although they are not visible in the raw data due to short period energy of the eruptive tremor and ambient seismic noise, VLP waveforms become clearly visible after filtering the broadband records below 0.1 Hz (see Fig. 4A). Such low-frequency signals are clearly distinct from high-frequency VT earthquakes observed at Piton de la Fournaise as illustrated in Supplementary Fig. S2. VLP events are characterized by decaying harmonic low-frequency oscillations with dominant periods near 20 s lasting for about 100 s. To investigate the corresponding particle motion, we

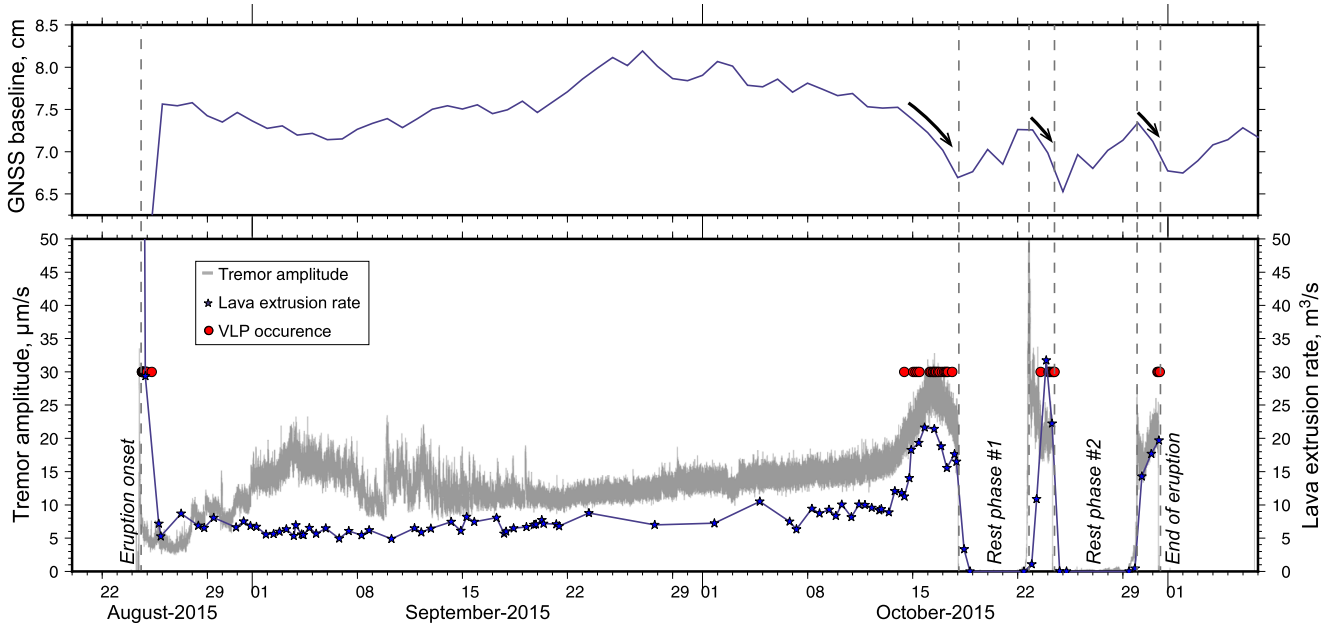

Fig. 3. Eruptive activity and VLP swarms. Top subfigure shows the variation of distance between GNSS stations SNE and DSR (cf., red triangles in Fig. 1A). The time-series is associated with an uncertainty of ~2 mm (cf., Fig. S1). In the bottom subfigure, the grey continuous lines indicate the time-evolution of the eruptive tremor amplitude in the 2-4 Hz passband. Blue stars indicate Time-Average lava Discharge Rate (TADR) derived from Moderate Resolution Imaging Spectroradiometer (MODIS) satellite data. Red circles indicate the detection times of VLP events. Grey dashed vertical lines indicate the onset, rest phases and end of the eruption. Black arrows highlight deflation episodes concomitant with VLP swarms in October 2015.

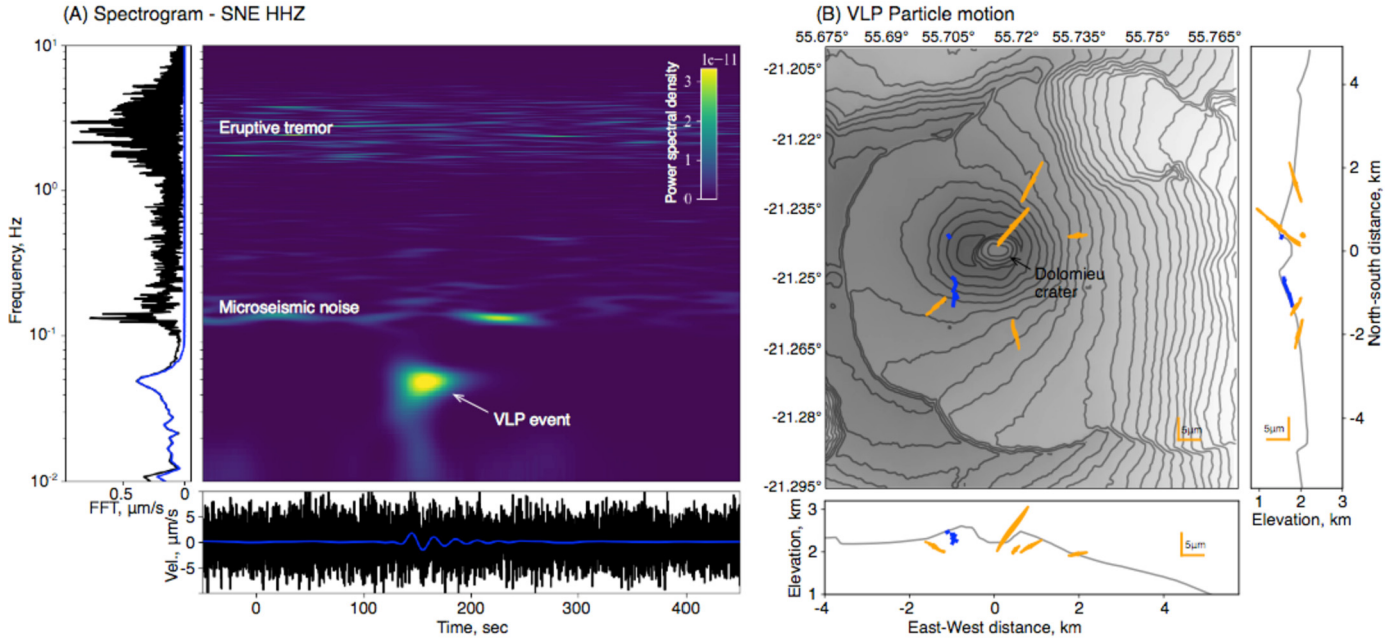

Fig. 4. VLP event on 24 August 2015 at 19:08:19 UTC. (**A**) Spectrogram at the seismic station SNE. Bottom subfigure shows the seismogram and Left plot shows the amplitude spectrum. Black lines correspond to the raw ground velocity record while blue lines are filtered in the 0.01-0.07 Hz passband. (**B**) Particle motions shown in orange for various seismic stations in map view, East-West and North-South cross-sections. Blue lines indicate the location of eruptive fissures.

corrected the horizontal orientation of broadband sensors using teleseismic records of distant earthquakes (see details in the supplementary Text S3). VLP signals depict radial polarization (Fig. 4B), suggesting a source location approximately 1 km below the western edge of the Dolomieu crater.

The VLP events were also recorded on tiltmeters located at the summit of the volcano. Fig. 5 shows a record from a Blum tiltmeter (Blum, 1963) that is co-located with the seismic station SNE (cf., Fig. 1A). As typically observed at Piton de la Fournaise, the tiltmeter data suggests a rapid inflation of the volcano summit at the onset of the magma injection followed by a deflation phase when the dike started to propagate toward the flank of the terminal cone (Peltier et al., 2005). We identify tilt offsets that are synchronous with VLP signals recorded on the broadband seismic stations. These tilt offsets are very small in magnitude (of the order of 10^{-2} microradian) and are observed in a radial direction that is consistent with the VLP waveform polarization shown in Fig. 4B.

To search for VLP signals in the seismic data, we used a template matching approach using a template catalog of 19 visually detected VLP events. These events occurred at different times of the eruption and were associated with different waveforms and frequency content (cf., Fig. S3). Detections were obtained by scanning vertical records from stations SNE and FJS after bandpass filtering between 0.02-0.07 Hz. We considered an average correlation threshold of 0.95 resulting in a total set of 48 detections (see supplementary Fig. S4 and S5). We then visually inspected the detected signals in comparison with long-period records at the GEOSCOPE station RER to discard teleseismic body-wave arrivals (VLP events were only recorded at stations located in the vicinity of the terminal cone). This resulted into a final set of 43 VLP events over the course of the eruption (between August 24 and October 31, 2015). The corresponding VLP waveforms are very similar and depict consistent polarization (see Fig. S4-S10). The detected VLP events are temporally clustered in four distinct swarms (Fig. 3) with inter-event times ranging from ~10 minutes at the onset of the eruption to several hours during the later VLP swarms (cf., Fig. S11). The first VLP swarm at the beginning of the eruption occurred synchronously with the decrease of lava fountain heights. The other three VLP swarms were detected before and during abrupt drops in magma extrusion rates that were observed before the two pauses in lava emissions and at the end of the eruption on October 31, 2015. All four swarms occurred when the eruptive tremor amplitude is large and when the lava extrusion rate is high (Fig. 3).

2.3. Dike resonance

We analyzed the source process of VLP events using six broadband stations in the vicinity of the terminal cone. Records were deconvolved to displacement and band-pass filtered at low frequency (0.03-0.1 Hz) to avoid any contamination by micro-seismic noise and eruptive tremor (cf., Fig. 4A). The forward problem can be written as (Aki and Richards, 2002):

$$u_i(\mathbf{x}, \boldsymbol{t}) = \int M_{pq}\, S(\tau)\; \boldsymbol{G_{ip,q}}(\mathbf{x}, \boldsymbol{t}; \boldsymbol{\xi}, \boldsymbol{\tau})\, d\tau \qquad (1)$$

where $u_i(\mathbf{x}, \boldsymbol{t})$ is the observed displacement at $(\mathbf{x}, \boldsymbol{t})$, $G_{ip,q}(\mathbf{x}, \boldsymbol{t}; \boldsymbol{\xi}, \boldsymbol{\tau})$ is the Earth response to a step function for a source at $(\boldsymbol{\xi}, \boldsymbol{\tau})$, M_{pq} is the moment tensor and $S(\tau)$ is a source time function (proportional to the moment rate). Our aim is to invert for the moment tensor elements (M_{pq}; i.e., the focal mechanism and magnitude), the source location ($\boldsymbol{\xi}$) and the shape of the moment-rate function ($S(\tau)$). A standard practice when dealing with tectonic earthquakes is to enforce positivity of $S(\tau)$ to avoid backward slip (i.e., slip in the direction opposite to the average fault motion; Duputel, 2022; Vallée et al., 2011). Such constraints do not apply to volcanic VLP events that are generally not produced by fault motion. This is the case in the present study, where near-field displacement waveforms shown in Fig. 6 exhibit long-period oscillations that cannot be fitted using positive definite moment rate functions. An approach used at volcanoes consists in describing the VLP source using a moment tensor and a single force, each component being associated with a source-time function to be estimated (e.g., Chouet, 1996; Kumagai, 2022; Ohminato et al., 1998). Although this method allows some flexibility in the source

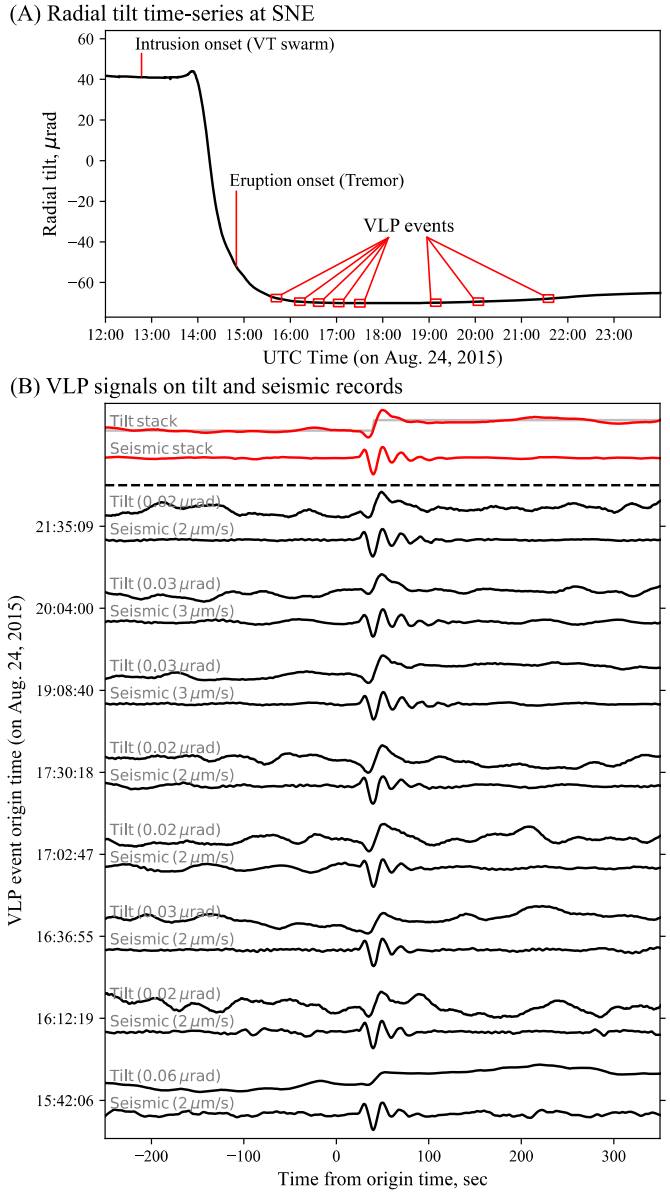

Fig. 5. Examples of VLP signals on tilt and seismic records. (**A**) Radial tilt time-series recorded at station SNE (see Fig. 1A). (**B**) Tilt steps and seismic signals observed for VLP events outlined with red rectangles in (A). Top traces in red are stacks of tilt and seismic records shown below. Tilt time-series are detrended and seismic signals are filtered in the 0.01-0.07 Hz passband after instrument correction. Ground velocity peak-to-peak amplitudes (in μm/sec) are indicated in gray on the left of each seismogram. Tilt steps (in μrad/sec) estimated using a simple step function are also indicated for each event. The corresponding average step function is shown in gray over the stack of tilt records (on top).

time history, it also involves a very large number of free parameters to be inverted for. To mitigate any tradeoff between model parameters, we used a simpler parameterization based on a moment tensor source with a damped oscillating source time function (Cesca et al., 2020):

$$S(t) \propto \exp\frac{-\pi t}{Q\,T_R}\sin\frac{2\pi t}{T_R} \qquad (2)$$

where the resonance period T_R and the quality factor Q are estimated by grid-search during the source inversion (the forward problem being linear for a given T_R and Q; see supplementary Text S5).

An example of VLP source model is shown in Fig. 6. The inverted moment tensor source is clearly non-double couple with a large isotropic component and a smaller CLVD deviatoric component (cf., Fig. 6A). This simple point source model fits the data very well (see Fig. 6C). This can likely be attributed to the fact that the observed VLP signals encompass wavelengths ranging from 50 to 70 km (assuming a P-wave velocity of 3.5 km/s) that is significantly greater than the source size (that cannot exceed a few kilometers given the dimensions of the volcano). To assess the corresponding source type, the root-mean-square (RMS) data misfit corresponding to each type of moment tensor source was derived using the approach described in Duputel and Rivera (2019). The optimum source-type (minimizing the RMS misfit) is close to a tensile crack (Fig. 6B). To confirm this result, we also imposed a pure crack source by fixing the ratio of eigenvalues of the seismic moment tensor and by searching for the optimum source orientation (the resulting solution corresponds to the "+Tensile Crack" source shown in Fig. 6B). Results indicate no significant deterioration of the data misfit compared to a full moment tensor inversion (see Fig. S12). The inverted source model is thus consistent with a tensile crack that is strongly dipping to the NE with opening/closing oscillations in the NE-SW direction at a resonance period $T_R \sim 20$ sec. This oscillating crack is located 1.2 km below the western edge of the Dolomieu crater, in rough agreement with the polarization of VLP signals shown in Fig. 4B. The source models obtained for the entire VLP catalog are presented in Fig. 7 and in Fig. S13. Overall, the source location and crack orientation are remarkably stable through the eruption. We note a slight change in source depth for the two last VLP swarms, occurring between 0.9 and 1.2 km below the summit while previous VLP occurred at depths of 1.1 - 1.2 km. The persistent localization of VLP events suggests a repeating and non-destructive source process. It is thus reasonable to consider that these VLP oscillations were caused by repetitive resonance within the magmatic dike feeding the eruption.

Although the oscillatory crack source is persistent through the eruption, we note a significant drift in its resonance period as a function of time. The comparison of the spectra of VLP events at the beginning and at the end of the eruptive sequence shows a change of the resonance period T_R of the crack-source oscillations (Fig. 8, Fig. S15 and supplementary Text S6). The first VLP swarm is associated with a rather constant resonance period $T_R \sim 20$ s, which gradually decreases to $T_R \sim 13$ s during the second swarm on October 14-17 prior to the first eruptive pause on October 18-22 and remains at this level until the end of the eruption on October 31. In addition to the change of resonance period, we also note a small decrease in the event magnitude (from Mw∼2.2 to Mw∼1.9) along with an initial increase in the quality factor Q followed by a decrease between the first and the second VLP swarm (Fig. S13).

3. Discussion and conclusion

We report previously undetected syn-eruptive VLP signals at Piton de la Fournaise volcano. We identify 43 VLP events during the August-October 2015 eruption that are temporally clustered in four distinct swarms at the beginning of the eruption and before abrupt drops in lava discharge. The analysis of VLP signals indicates that these signals were most likely generated by the resonance of the magmatic dike feeding the eruption. While the location and orientation of the resonator source are remarkably persistent over time, there is a change in resonance period, shifting from $T_R \sim 20$ s at the beginning of the eruption to $T_R \sim 13$ s at the end of the eruption. As discussed below, this change most likely represents variations in the physical properties of the dike feeding the eruption.

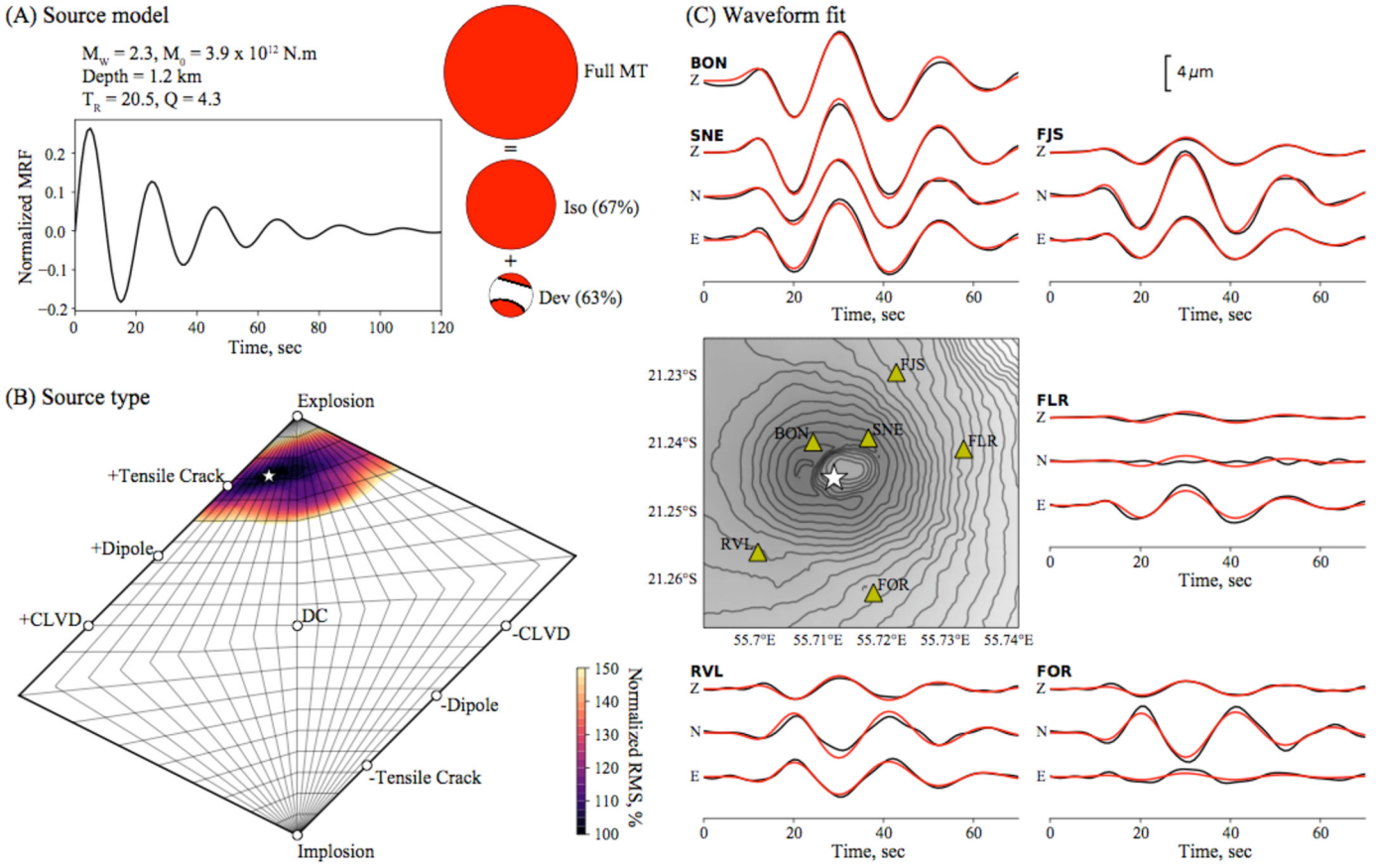

Fig. 6. Source analysis of the VLP event on 24 August 2015 at 19:08:19 UTC. (**A**) Moment tensor solution (decomposed into isotropic and deviatoric components on the right) obtained by considering a damped oscillating source-time function (characterized by a resonance period T_R and a quality factor Q). Beachballs diagrams are shown for the lower-hemisphere. (**B**) Source type plot. Colors indicate the Normalized RMS misfit for different source-types. White star indicates the optimum source type (minimizing RMS misfit). (**C**) Comparison between observed (black) and predicted (red) waveforms. The map indicates the source location (white star) and seismic stations (yellow triangles). The source model is consistent with an oscillating tensile crack with a dip angle of 77° and a strike of 286°, which fits the data as well as a full moment tensor (cf., Fig. S12).

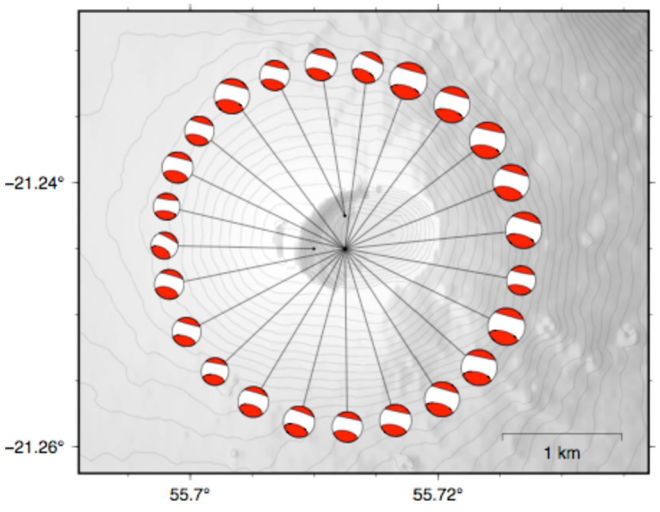

Fig. 7. VLP source mechanisms during the August 2015 eruption. We only show the deviatoric part of the moment tensor solutions to highlight the orientation of the crack source. The (lower hemisphere) focal mechanisms and source locations are very consistent between VLP events. Source depth are also similar, ranging from 0.9 to 1.2 km. Only three VLP events have a slightly different horizontal location, which probably results from a limited resolution at low frequency (0.01-0.03 Hz).

To interpret changes in resonance period, we consider here that the magma dike can be represented by a fluid-filled rectangular crack embedded in an elastic medium. Numerical simulations introduced initially by Chouet (1986) show that fluid pressure perturbations in such a crack induce resonant oscillations of the crack wall. These oscillations can be decomposed into different modes m whose resonance periods (T_R^m) are primarily sensitive to the dimensions of the crack (length L, width W and thickness d), the bulk modulus of the magma (b) and its density (ρ) (Maeda and Kumagai, 2017):

$$T_R^m = \frac{2W}{(m-1)}\sqrt{\frac{\rho(1+2\varepsilon^m C)}{b}} \quad (3)$$

where ε^m is an empirical constant defined as $\varepsilon^m = W(1 - 4\gamma W/3mL)/3mL$ and C is the crack stiffness $C = (b/\mu)(W/d)$ with $\gamma = 0.22$ and μ the shear modulus of the magma (cf., supplementary Text S7).

Because variations in gas content can largely impact magma properties (i.e., magma bulk modulus and density in equation (3); Huppert and Woods, 2002), they can induce changes in the resonance period of the crack. However, the observed change of T_R would require a very large reduction of the gas volume fraction from 100% at the beginning of the eruption to 0% at the end of the eruption (see Fig. S16). This scenario is unrealistic, considering other constraints on gas exsolution at Piton de la Fournaise. Previous studies have demonstrated that gas emissions are largely dominated by H_2O exsolved at very shallow depth (Allard et al., 2011; Lénat et al., 1989). Using recent analyses of dissolved water

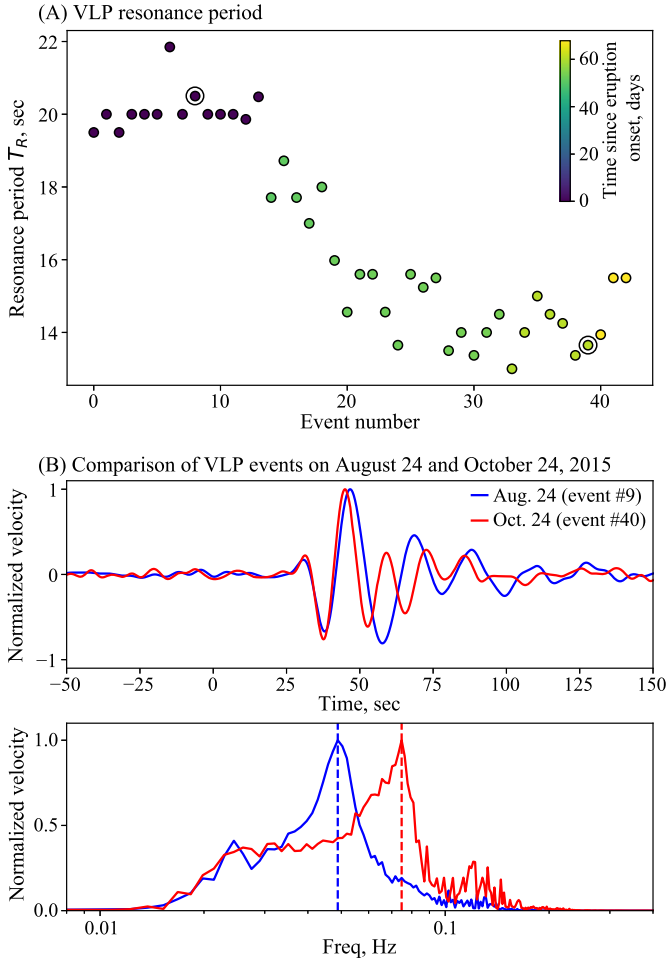

Fig. 8. Time-evolution of the VLP resonance periods. (**A**) Time-evolution of the resonance period of VLP events. Colors indicate the time in days since the eruption onset (on August 24, 2015). (**B**) Examples of VLP events recorded at station SNE on August 24 and October 24, 2015. Ground velocity is shown on top and the corresponding amplitude spectrum is shown below. Records are filtered in the 0.02-0.1 Hz passband after instrument correction.

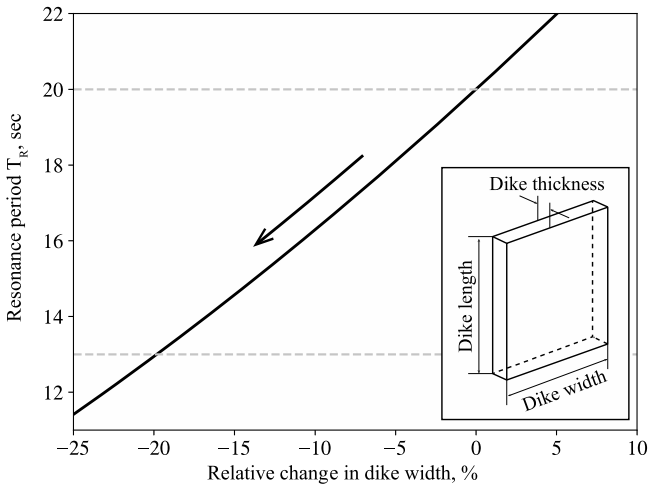

Fig. 9. Change in the resonance period of a magma-filled dike as a function of the dike width. Horizontal dashed grey lines indicate resonance periods $T_R = 20$ sec and $T_R = 13$ sec, observed at the beginning and at the end of the sequence, respectively. We show relative changes in dike width with respect to the width predicted for each mode for a resonance period $T_R = 20$ sec. Such normalization allows us to mitigate any dependency on mode number, dike length and thickness. Inset on the lower right corner indicate the dike geometry considered in the empirical analytical calculations.

in glass inclusions and matrices (Muro et al., 2016), we have estimated the evolution of gas content in the magma as a function of depth (cf., supplementary Text S8). Results indicate negligible vapor content at the VLP source depth (∼1 km) and an average gas volume fraction smaller than a few percent when averaging over the entire dike length (Fig. S17). This suggests that only small variations of gas content are possible, which cannot explain the observed change in the resonance period of the dike. Besides gas content, changes in magma chemistry and temperature can impact the magma density and therefore induce variations of resonance period (Lesher and Spera, 2015). The second VLP swarm was preceded by an increase in MgO content, which is possibly associated to the incoming of magma from deeper storage zones (Coppola et al., 2017). However, the observed change of resonance period would require an unrealistic decrease in magma density of about 60% (cf., Fig. S18). While we do dismiss the possibility of variations in magma chemistry or gas content, the estimates provided above indicate that these factors cannot fully explain the magnitude of the observed shift in resonance period.

In order to explain the observed changes in resonance properties, it is necessary to explore variations in the physical properties of the dike throughout the eruption. Fig. 9 shows the crack resonance period T_R as a function of the relative change in dike width ($\delta W/W$). We examined variations in terms of $\delta W/W$ because it removes any dependency on the mode number, dike length and dike thickness (cf., Fig. S19 and supplementary Text S7). The transition from $T_R \sim 20$ s to $T_R \sim 13$ s can then be attributed to a ∼20% decrease in the dike width. Assuming that we are dealing with the fundamental mode of transverse oscillations in a dike of length 2300 m and thickness 1 m, this translates to a reduction of the dike width from 1440 m to 1150 m. These estimates rely on the assumption that magma behaves as an inviscid fluid (Maeda and Kumagai, 2017). To evaluate the impact of viscous flow, we additionally employed the model proposed by Lipovsky and Dunham (2015) to estimate the time evolution of the dike width and magma viscosity. This approach relies on the resonance periods and quality factors determined for each VLP event, as described in supplementary Text S7. Results presented in Fig. S20 are globally consistent with estimates derived from Maeda and Kumagai (2017) with a reduction of the dike width from 1300 m to 1000 m (i.e., a decrease of ∼20%). The estimated magma viscosity increases toward the end of the eruption with values around 200 to 400 Pa.s, consistent with previous estimates at Piton de la Fournaise volcano (e.g., Harris et al., 2017; Villeneuve et al., 2008). The contraction of the dike size, supported by both models, is consistent with field observations showing that the eruption began with several elongated eruptive fissures and later focused on a single vent (Fig. 1, Movies M1 and M2).

Evolution of erupting dikes have been investigated in various theoretical and experimental studies (e.g., Bruce and Huppert, 1989; Pansino et al., 2019; Taisne and Tait, 2011; Wylie et al., 1999). As they propagate and increase their surface area, dikes become increasingly susceptible to heat loss via conduction. When the incoming magma is very hot and the flow rate is high, thermal erosion occurs on the dike walls. On the other hand, when the flow rate is low, heat transfer to the surrounding rock leads to magma solidification, which can reduce the width of the dike. According to the time-evolution of the resonance period (Fig. 8 and Fig. S21), the reduction of the dike width at depth occurred mainly over a few days during the second VLP swarm. As shown in Fig. 3 and Fig. S22, this change was associated by a rapid summit deflation that can be modeled by the contraction of the dike above the magma reservoir. This shortening of the dike was then accompanied by a decrease in magma flux just before a sudden drop in

lava discharge marking the first eruptive pause of October 18-22, 2015. This suggests that partial solidification of the magmatic dike during the eruption induced a decrease of the magma flux. Such channelization accompanied with a decrease of the magma flux could be at the origin of the unstable on-and-off eruptive phases observed at the end of the eruption as suggested by laboratory experiments (Pansino et al., 2019).

Although this is a first time observation at Piton de la Fournaise, VLP signals resulting from the resonance of magmatic dikes and conduits have been observed at several volcanoes, with oscillation properties providing information about the dynamics of subsurface magma transport (Chouet and Matoza, 2013; Crozier and Karlstrom, 2022; Kumagai et al., 2003; Legrand and Perton, 2022; Niu and Song, 2021). The lack of previous VLP detections at Piton de la Fournaise results from two main factors. First, the broadband seismic network was very sparse prior to 2010. Broadband stations started to be deployed at the end of the year 2009 (Brenguier, 2014) and were integrated to the permanent monitoring network in 2011 (Observatoire Volcanologique Du Piton De La Fournaise (OVPF) and Institut De Physique Du Globe De Paris (IPGP), 2008). Second, syn-eruptive VLP signals can be difficult to identify on raw data as they can be hidden by the eruptive tremor. Using a template matching approach similar to the one employed during the August-October 2015 eruption, we analyzed continuous seismic records between 2014 and 2015. Results indicate that VLP events occurred during all five eruptions of this time-period. Even though details in the waveforms are different, detected signals have similar properties such as enhanced long-period radial polarization pointing below the volcano summit (Fig. S23-S29).

This work encourages a systematic detection of VLP signals in order to monitor changes in magma transport during volcanic eruptions. For all eruptions between 2014 and 2015 at Piton de la Fournaise, VLP events were detected primarily when the lava extrusion rate is rapidly decreasing (Fig. S30). This is particularly evident for the three later VLP swarms of the August-October 2015 eruptions, which systematically occurred before sudden drops in lava emissions. These swarms were accompanied by rapid summit deflations (Fig. 3), corresponding to the contraction of the dike above the shallow reservoir (see Fig. S20 and Fig. S22). Although the excitation process of the dike resonance is currently unknown, this suggests that VLP events are associated with rapid pressure variations in the volcano plumbing system. The detection of VLP events is therefore useful for monitoring purposes because they indicate changes in the magma flow that may lead to a permanent or temporary cessation of lava emissions. This is particularly interesting for long-lived eruptions with complicated time-evolution whose end is difficult to anticipate.

CRediT authorship contribution statement

Zacharie Duputel: Conceptualization, Data curation, Formal analysis, Funding acquisition, Investigation, Methodology, Project administration, Software, Supervision, Validation, Visualization, Writing – original draft. **Valérie Ferrazzini:** Conceptualization, Data curation, Formal analysis, Investigation, Methodology, Resources, Software, Supervision, Validation, Visualization, Writing – review & editing. **Cyril Journeau:** Methodology, Software, Writing – review & editing. **Philippe Catherine:** Data curation. **Philippe Kowalski:** Data curation. **Aline Peltier:** Data curation, Writing – review & editing.

Declaration of competing interest

The authors declare that they have no known competing financial interests or personal relationships that could have appeared to influence the work reported in this paper.

Data availability

Data is freely available (DOI and links provided in the manuscript).

Acknowledgements

We thank Luis Rivera, Olivier Lengliné, Oryaelle Chevrel and Dimitri Zigone for helpful discussion. We thank Martin Vallée for his help in estimating the orientation of broadband seismological stations. We are also thankful to Diego Coppola for providing TADR measurements. We thank Simone Cesca and two anonymous reviewers for their comments that allowed us to improve the manuscript. This project was supported by the European Research Council (ERC, under the European Union's Horizon 2020 research and innovation program under grant agreement No. 805256). OVPF data is freely available through the VOLOBSIS (http://volobsis.ipgp.fr) and RESIF data portals (http://resif.fr).

Appendix A. Supplementary material

Supplementary material related to this article can be found online at https://doi.org/10.1016/j.epsl.2023.118323.

References

Aki, K., Ferrazzini, V., 2000. Seismic monitoring and modeling of an active volcano for prediction (vol 105, pg 16,617, 2000). J. Geophys. Res. 105, 16617–16640.

Aki, K., Richards, P.G., 2002. Quantitative Seismology, 2nd ed. University Science Books, Sausalito, CA.

Allard, P., La Spina, A., Tamburello, G., Aiuppa, A., Muro, A.D., Staudacher, T., 2011. First Measurements of Magmatic Gas Composition and FLuxes during an Eruption (October 2010) of Piton de La Fournaise Hot Spot Volcano, La Reunion Island. Geophysical Research Abstracts 13, EGU2011-13182. Geophysical Research Abstracts, EGU General Assembly GMPV5, 13182.

Aster, R., Mah, S., Kyle, P., McIntosh, W., Dunbar, N., Johnson, J., Ruiz, M., McNamara, S., 2003. Very long period oscillations of Mount Erebus Volcano. J. Geophys. Res., Solid Earth 108. https://doi.org/10.1029/2002JB002101.

Beauducel, F., Peltier, A., Villié, A., Suryanto, W., 2020. Mechanical imaging of a volcano plumbing system from GNSS unsupervised modeling. Geophys. Res. Lett. 47, e2020GL089419. https://doi.org/10.1029/2020GL089419.

Blum, P.-A., 1963. Contribution à l'étude des variations de la verticale en un lieu. Ann. Geophys. 19, 215–243.

Bonny, E., Wright, R., 2017. Predicting the end of lava flow-forming eruptions from space. Bull. Volcanol. 79, 52. https://doi.org/10.1007/s00445-017-1134-8.

Brenguier, F., 2014. UNDERVOLC experiment, 2009-2011, code YA (understanding volcanic processes). https://doi.org/10.15778/RESIF.YA2009.

Bruce, P.M., Huppert, H.E., 1989. Thermal control of basaltic fissure eruptions. Nature 342, 665–667. https://doi.org/10.1038/342665a0.

Cesca, S., Letort, J., Razafindrakoto, H.N.T., Heimann, S., Rivalta, E., Isken, M.P., Nikkhoo, M., Passarelli, L., Petersen, G.M., Cotton, F., Dahm, T., 2020. Drainage of a deep magma reservoir near Mayotte inferred from seismicity and deformation. Nat. Geosci. 13, 87–93. https://doi.org/10.1038/s41561-019-0505-5.

Chevrel, M.O., Favalli, M., Villeneuve, N., Harris, A.J.L., Fornaciai, A., Richter, N., Derrien, A., Boissier, P., Di Muro, A., Peltier, A., 2021. Lava flow hazard map of Piton de la Fournaise volcano. Nat. Hazards Earth Syst. Sci. 21, 2355–2377. https://doi.org/10.5194/nhess-21-2355-2021.

Chevrel, M.O., Harris, A., Peltier, A., Villeneuve, N., Coppola, D., Gouhier, M., Drenne, S., 2022. Volcanic crisis management supported by near real-time lava flow hazard assessment at Piton de la Fournaise, La Réunion. Volcanica 5, 313–334. https://doi.org/10.30909/vol.05.02.313334.

Chouet, B., 1986. Dynamics of a fluid-driven crack in three dimensions by the finite difference method. J. Geophys. Res., Solid Earth 91, 13967–13992. https://doi.org/10.1029/JB091iB14p13967.

Chouet, B.A., 1996. New Methods and Future Trends in Seismological Volcano Monitoring. Springer, Berlin, Heidelberg, pp. 23–97.

Chouet, B.A., Matoza, R.S., 2013. A multi-decadal view of seismic methods for detecting precursors of magma movement and eruption. J. Volcanol. Geotherm. Res. 252, 108–175.

Coppola, D., Piscopo, D., Staudacher, T., Cigolini, C., 2009. Lava discharge rate and effusive pattern at Piton de la Fournaise from MODIS data. J. Volcanol. Geotherm. Res. 184, 174–192.

Coppola, D., Di Muro, A., Peltier, A., Villeneuve, N., Ferrazzini, V., Favalli, M., Bachèlery, P., Gurioli, L., Harris, A.J.L., Moune, S., Vlastélic, I., Galle, B., Arellano, S., Aiuppa, A., 2017. Shallow system rejuvenation and magma discharge trends at Piton de la Fournaise volcano (La Réunion Island). Earth Planet. Sci. Lett. 463, 13–24. https://doi.org/10.1016/j.epsl.2017.01.024.

Crozier, Josh, Karlstrom, L., 2022. Evolving magma temperature and volatile contents over the 2008–2018 summit eruption of Kīlauea Volcano. Sci. Adv. 8, eabm4310. https://doi.org/10.1126/sciadv.abm4310.

Dumont, Q., Cayol, V., Froger, J.-L., Peltier, A., 2022. 22 years of satellite imagery reveal a major destabilization structure at Piton de la Fournaise. Nat. Commun. 13, 2649. https://doi.org/10.1038/s41467-022-30109-w.

Duputel, Z., 2022. Co-seismic phase: imaging the seismic rupture. In: The Seismic Cycle. John Wiley & Sons, Ltd, pp. 39–77.

Duputel, Z., Rivera, L., 2019. The 2007 caldera collapse of Piton de la Fournaise volcano: source process from very-long-period seismic signals. Earth Planet. Sci. Lett. 527, 115786. https://doi.org/10.1016/j.epsl.2019.115786.

Duputel, Z., Lengliné, O., Ferrazzini, V., 2019. Constraining spatiotemporal characteristics of magma migration at Piton De La Fournaise volcano from pre-eruptive seismicity. Geophys. Res. Lett. 46, 119–127. https://doi.org/10.1029/2018GL080895.

Duputel, Z., Ferrazzini, V., Lengliné, O., Michon, L., Fontaine, F.R., Massin, F., 2021. Seismicity of La Réunion island. C. R. Géosci. 353, 237–255. https://doi.org/10.5802/crgeos.77.

Fontaine, F.R., Roult, G., Hejrani, B., Michon, L., Ferrazzini, V., Barruol, G., Tkalčić, H., Di Muro, A., Peltier, A., Reymond, D., Staudacher, T., Massin, F., 2019. Very- and ultra-long-period seismic signals prior to and during caldera formation on La Réunion Island. Sci. Rep. 9, 8068. https://doi.org/10.1038/s41598-019-44439-1.

Fukushima, Y., Cayol, V., Durand, P., Massonnet, D., 2010. Evolution of magma conduits during the 1998–2000 eruptions of Piton de la Fournaise volcano, Réunion Island. J. Geophys. Res., Solid Earth 115. https://doi.org/10.1029/2009JB007023.

Got, J.-L., Peltier, A., Staudacher, T., Kowalski, P., Boissier, P., 2013. Edifice strength and magma transfer modulation at Piton de la Fournaise volcano. J. Geophys. Res., Solid Earth 118, 5040–5057. https://doi.org/10.1002/jgrb.50350.

Harris, A.J.L., Villeneuve, N., Di Muro, A., Ferrazzini, V., Peltier, A., Coppola, D., Favalli, M., Bachèlery, P., Froger, J.L., Gurioli, L., Moune, S., Vlastélic, I., Galle, B., Arellano, S., 2017. Effusive crises at Piton de la Fournaise 2014–2015: a review of a multi-national response model. J. Appl. Volcanol. 6, 11. https://doi.org/10.1186/s13617-017-0062-9.

Hibert, C., Mangeney, A., Polacci, M., Muro, A.D., Vergniolle, S., Ferrazzini, V., Peltier, A., Taisne, B., Burton, M., Dewez, T., Grandjean, G., Dupont, A., Staudacher, T., Brenguier, F., Kowalski, P., Boissier, P., Catherine, P., Lauret, F., 2015. Toward continuous quantification of lava extrusion rate: results from the multidisciplinary analysis of the 2 January 2010 eruption of Piton de la Fournaise volcano, La Réunion. Earth Space Sci. 120, 3026–3047. https://doi.org/10.1002/2014JB011769.

Huppert, H.E., Woods, A.W., 2002. The role of volatiles in magma chamber dynamics. Nature 420, 493–495. https://doi.org/10.1038/nature01211.

Jones, T.J., Llewellin, E.W., Houghton, B.F., Brown, R.J., Vye-Brown, C., 2017. Proximal lava drainage controls on basaltic fissure eruption dynamics. Bull. Volcanol. 79, 81. https://doi.org/10.1007/s00445-017-1164-2.

Journeau, C., Shapiro, N.M., Seydoux, L., Soubestre, J., Ferrazzini, V., Peltier, A., 2020. Detection, classification, and location of seismovolcanic signals with multicomponent seismic data: example from the Piton de La Fournaise volcano (La Réunion, France). J. Geophys. Res., Solid Earth 125, e2019JB019333. https://doi.org/10.1029/2019JB019333.

Keating, G.N., Valentine, G.A., Krier, D.J., Perry, F.V., 2008. Shallow plumbing systems for small-volume basaltic volcanoes. Bull. Volcanol. 70, 563–582. https://doi.org/10.1007/s00445-007-0154-1.

Kumagai, H., 2006. Temporal evolution of a magmatic dike system inferred from the complex frequencies of very long period seismic signals. J. Geophys. Res., Solid Earth 111. https://doi.org/10.1029/2005JB003881.

Kumagai, H., 2022. Source Quantification of Volcanic-Seismic Signals. In: Tilling, R.I. (ed.). Springer US, New York, NY, pp. 425–467.

Kumagai, H., Miyakawa, K., Negishi, H., Inoue, H., Obara, K., Suetsugu, D., 2003. Magmatic dike resonances inferred from very-long-period seismic signals. Science. https://doi.org/10.1126/science.1081195.

Legrand, D., Perton, M., 2022. What are VLP signals at Stromboli volcano? J. Volcanol. Geotherm. Res. 421, 107438. https://doi.org/10.1016/j.jvolgeores.2021.107438.

Lénat, J.-F., Bachèlery, P., Bonneville, A., Tarits, P., Cheminée, J.-L., Delorme, H., 1989. The December 4, 1983 to February 18, 1984 eruption of Piton de la Fournaise (La Reunion, Indian Ocean): description and interpretation. J. Volcanol. Geotherm. Res. 36, 87–112. https://doi.org/10.1016/0377-0273(89)90007-3.

Lesher, C.E., Spera, F.J., 2015. Thermodynamic and transport properties of silicate melts and magma. In: Sigurdsson, H. (Ed.), The Encyclopedia of Volcanoes, second edition. Academic Press, Amsterdam, pp. 113–141 (Chapter 5).

Liang, C., Crozier, J., Karlstrom, L., Dunham, E.M., 2020. Magma oscillations in a conduit-reservoir system, application to very long period (VLP) seismicity at basaltic volcanoes: 2. Data inversion and interpretation at Kīlauea volcano. J. Geophys. Res., Solid Earth 125, e2019JB017456. https://doi.org/10.1029/2019JB017456.

Lipovsky, B.P., Dunham, E.M., 2015. Vibrational modes of hydraulic fractures: inference of fracture geometry from resonant frequencies and attenuation. J. Geophys. Res., Solid Earth 120, 1080–1107. https://doi.org/10.1002/2014JB011286.

Maeda, Y., Kumagai, H., 2017. A generalized equation for the resonance frequencies of a fluid-filled crack. Geophys. J. Int. 209, 192–201. https://doi.org/10.1093/gji/ggx019.

Muro, A.D., Métrich, N., Allard, P., Aiuppa, A., Burton, M., Galle, B., Staudacher, T., 2016. Magma degassing at Piton de la Fournaise volcano. In: Active Volcanoes of the Southwest Indian Ocean. Springer, pp. 203–222.

Niu, J., Song, T.-R.A., 2021. Episodic transport of discrete magma batches beneath Aso volcano. Nat. Commun. 12, 1–12. https://doi.org/10.1038/s41467-021-25883-y.

Observatoire Volcanologique Du Piton De La Fournaise (OVPF), Institut De Physique Du Globe De Paris (IPGP), 2008. Seismic, tiltmeter, extensometer, magnetic and weather permanent networks on Piton de la Fournaise volcano and La Réunion. https://doi.org/10.18715/REUNION.PF.

Ohminato, T., Chouet, B.A., Dawson, P., Kedar, S., 1998. Waveform inversion of very long period impulsive signals associated with magmatic injection beneath Kilauea volcano, Hawaii. J. Geophys. Res., Solid Earth 103, 23839–23862. https://doi.org/10.1029/98JB01122.

Pansino, S., Emadzadeh, A., Taisne, B., 2019. Dike channelization and solidification: time scale controls on the geometry and placement of magma migration pathways. J. Geophys. Res., Solid Earth 124, 9580–9599. https://doi.org/10.1029/2019JB018191.

Peltier, A., Ferrazzini, V., Staudacher, T., Bachèlery, P., 2005. Imaging the dynamics of dyke propagation prior to the 2000–2003 flank eruptions at Piton de La Fournaise, Reunion Island. Geophys. Res. Lett. 32, L22302. https://doi.org/10.1029/2005GL023720.

Peltier, A., Massin, F., Bachelery, P., Finizola, A., 2012. Internal structure and building of basaltic shield volcanoes: the example of the Piton de La Fournaise terminal cone (La Reunion). Bull. Volcanol. 74, 1881–1897. https://doi.org/10.1007/s00445-012-0636-7.

Peltier, A., Ferrazzini, V., Di Muro, A., Kowalski, P., Villeneuve, N., Richter, N., Chevrel, O., Froger, J.L., Hrysiewicz, A., Gouhier, M., Coppola, D., Retailleau, L., Beauducel, F., Gurioli, L., Boissier, P., Brunet, C., Catherine, P., Fontaine, F., Lauret, F., Garavaglia, L., Lebreton, J., Canjamale, K., Desfete, N., Griot, C., Harris, A., Arellano, S., Liuzzo, M., Gurrieri, S., Ramsey, M., 2020. Volcano crisis management at Piton de la Fournaise (La Réunion) during the Covid-19 lockdown. Seismol. Res. Lett. 92, 38–52. https://doi.org/10.1785/0220200212.

Peltier, A., Chevrel, M.O., Harris, A.J.L., Villeneuve, N., 2022. Reappraisal of gap analysis for effusive crises at Piton de la Fournaise. J. Appl. Volcanol. 11, 2. https://doi.org/10.1186/s13617-021-00111-w.

Richter, D.H., Eaton, J.P., Murata, K.J., Ault, W.U., Krivoy, H.L., 1970. Chronological narrative of the 1959-60 eruption of Kilauea volcano, Hawaii. Professional Paper No. 537- E. U.S. Geological Survey.

Roult, G., Peltier, A., Taisne, B., Staudacher, T., Ferrazzini, V., Di Muro, A., 2012. A new comprehensive classification of the Piton de la Fournaise activity spanning the 1985–2010 period. Search and analysis of short-term precursors from a broad-band seismological station. J. Volcanol. Geotherm. Res. 241–242, 78–104. https://doi.org/10.1016/j.jvolgeores.2012.06.012.

Sapin, M., Hirn, A., Lépine, J.-C., Nercessian, A., 1996. Stress, failure and fluid flow deduced from earthquakes accompanying eruptions at Piton de la Fournaise volcano. J. Volcanol. Geotherm. Res. 70, 145–167. https://doi.org/10.1016/0377-0273(95)00043-7.

Smittarello, D., Cayol, V., Pinel, V., Peltier, A., Froger, J.L., Ferrazzini, V., 2019. Magma propagation at Piton de la Fournaise from joint inversion of InSAR and GNSS. J. Geophys. Res., Solid Earth 124, 1361–1387. https://doi.org/10.1029/2018JB016856.

Staudacher, T., Peltier, A., 2016. Ground Deformation at Piton de la Fournaise, a Review From 20 Years of GNSS Monitoring. In: Bachelery, P., Lenat, J.F., Di Muro, A., Michon, L. (Eds.), Active Volcanoes of the Southwest Indian Ocean. Active Volcanoes of the World. Springer, Berlin, Heidelberg. https://doi-org.insu.bib.cnrs.fr/10.1007/978-3-642-31395-0er_15.

Taisne, B., Tait, S., 2011. Effect of solidification on a propagating dike. J. Geophys. Res., Solid Earth 116. https://doi.org/10.1029/2009JB007058.

Taisne, B., Brenguier, F., Shapiro, N.M., Ferrazzini, V., 2011. Imaging the dynamics of magma propagation using radiated seismic intensity. Geophys. Res. Lett. 38, L04304. https://doi.org/10.1029/2010GL046068.

Vallée, M., Charléty, J., Ferreira, A.M.G., Delouis, B., Vergoz, J., 2011. SCARDEC: a new technique for the rapid determination of seismic moment magnitude, focal mechanism and source time functions for large earthquakes using body-wave deconvolution. Geophys. J. R. Astron. Soc. 184, 338–358. https://doi.org/10.1111/j.1365-246X.2010.04836.x.

Villeneuve, N., Neuville, D.R., Boivin, P., Bachèlery, P., Richet, P., 2008. Magma crystallization and viscosity: a study of molten basalts from the Piton de la Fournaise volcano (La Réunion island). In: 8th Silicate Melt Workshop. Chem. Geol. 256, 242–251. https://doi.org/10.1016/j.chemgeo.2008.06.039.

Wadge, G., 1981. The variation of magma discharge during basaltic eruptions. J. Volcanol. Geotherm. Res. 11, 139–168. https://doi.org/10.1016/0377-0273(81)90020-2.

Witt, T., Walter, T.R., Müller, D., Guðmundsson, M.T., Schöpa, A., 2018. The relationship between lava fountaining and vent morphology for the 2014–2015 Holuhraun eruption, Iceland, analyzed by video monitoring and topographic mapping. Front. Earth Sci. 6.

Wylie, J.J., Helfrich, K.R., Dade, B., Lister, J.R., Salzig, J.F., 1999. Flow localization in fissure eruptions. Bull. Volcanol. 60, 432–440. https://doi.org/10.1007/s004450050243.

Zecevic, M., De Barros, L., Bean, C.J., O'Brien, G.S., Brenguier, F., 2013. Investigating the source characteristics of long-period (LP) seismic events recorded on Piton de la Fournaise volcano, La Réunion. J. Volcanol. Geotherm. Res. 258, 1–11. https://doi.org/10.1016/j.jvolgeores.2013.04.009.